Stress-guided self-assembly in Dutcher films

Gavin A. Buxton and Nigel Clarke

Department of Chemistry, University of Durham, Durham DH1 3LE, United Kingdom

(Received 28 November 2005; published 10 April 2006)

Dutcher films consist of a layer of liquid sandwiched between two solid capping layers and can spontaneously self-assemble to form corrugated surfaces. The interplay between the attractive van der Waals forces across the film, and the elastic forces due to the deformation of the capping layers, produces well-defined periodic undulations. We show how computer simulations can capture both the formation of undulations in Dutcher films and the correct periodicity. Furthermore, we simulate Dutcher films which are either compressed or stretched, resulting in the promotion or suppression of undulation growth. In this manner, applied deformations can be shown to guide the self-assembly process in Dutcher films and result in the formation of highly oriented surface corrugations over large distances.

Optical components [1], scattering elements in light emitting diodes [2], and substrates for tissue growth [3] are just some of the potential applications for corrugated thin films. Here, we concentrate on the spontaneous formation of surface undulations in Dutcher films [4–6]; thin trilayer systems consisting of a liquid layer sandwiched in between two solid capping layers. Surface undulations form in Dutcher films with a characteristic wavelength depending on the interplay between the attractive van der Waals forces across the film and the elastic forces due to the deformation of the solid capping layers. In order to tailor the surface of these films towards specific applications it is necessary to control both the anisotropy and the long-range order of the surface undulations. We show how computer simulations can capture the spontaneous formation of surface undulations in Dutcher films and, furthermore, how the application of relatively small strain fields can result in the formation of desirable patterns with acceptable regularity.

Surface undulations can be created in a number of systems and in a variety of ways. For example, in bilayer systems large compressive stresses can arise upon cooling due to a mismatch in thermal expansion coefficients between the different layers [7]. These compressive stresses can then lead to the buckling of the top layer and the formation of surface undulations. Yoo *et al.* [8] has shown how placing an elastomeric mold on top of such a surface can result in a pattern transfer from the mold to the buckling capping layer. An alternative method for controlling the undulations in these systems is to apply external compressive stresses. Ohzono *et al.* [9] applied relatively large uniaxial compressive strains (7%) in order to "orient" the buckling. However, it should be noted that the application of compressive strains of this magnitude can result in the formation of buckling instabilities in their own right [10]. Recently, the thermal expansion mismatch between the core and shell in Ag core/SiOx shell microstructures was found to result in complex patterns due to both the shell buckling and the spherical geometry [11].

Buckling instabilities can also arise due to the confinement of osmotically swollen polymer films [12] or possibly as a consequence of an acoustic Casimir effect [13]. However, buckling instabilities in "ultrathin" films are more commonly associated with van der Waals interactions across the film [4–6,14]. In Dutcher films, and thin films in general, attractive van der Waals, or dispersion, forces can amplify interfacial thermal fluctuations [15]. That is, the van der Waals forces across the film cause the spontaneous growth of surface deformations. However, deforming the solid capped surfaces is energetically unfavorable. It is this complex interplay between van der Waals interactions and elastic deformations which results in a phenomena known as "spinodal deformation" [14]. Thermal fluctuations on the surface of the film can grow if the wavelength of the instability is large enough. Furthermore, the exponential growth of these deformations is fastest for a given wavelength (essentially *selecting* this periodicity in the system). Typically, a lateral morphology consisting of parallel domains of peaks and troughs is observed locally, whilst globally the deformation pattern remains isotropic [4–6,14]. The orientation of surface corrugations can be locally ordered at defects or cracks [6,14], however, it would be advantageous to impose long-range order and uniformity on to these systems.

In order to capture the formation of surface undulations in Dutcher films we augment a thin film equation [16,17], derived from the Navier-Stokes equations, with pressures from the elastic deformation of the capping layers [18]. The thin film equation has been successfully applied to capture the dewetting phenomena in thin liquid films [16,19,20]. Besides modeling dewetting behavior in quantitative agreement with the experiments [21], the thin film equation has been successfully applied to dewetting on chemically heterogeneous substrates [22], dewetting with local density fluctuations [23], and the dewetting of phase separating blends [24].

It is assumed that the film thickness is large enough that continuum fluid and elasticity theories are applicable, yet small enough that van der Waals forces play a part. We begin with the Navier-Stokes equations under long-wave approximations. That is, we assume the film thickness is much smaller than the characteristic wavelength of undulations in the lateral plane. Under this condition the Navier-Stokes equations can lead to the following boundary layer equations [17,25]:
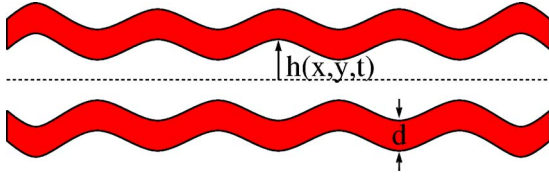
FIG. 1. (Color online) Schematic of a thin polymer trilayer film. The thickness of the fluid layer is $2h(x,y,t)$ and the thickness of both the upper and lower solid capping layers is d.

$$\mu \frac{\partial^2 v_x}{\partial z^2} = \frac{\partial P}{\partial x}, \quad \mu \frac{\partial^2 v_y}{\partial z^2} = \frac{\partial P}{\partial y}, \quad (1)$$

where $\mathbf{v}$ is the fluid velocity, P is the pressure acting on the film surface, and μ is the fluid viscosity. The mass-conserving kinematic equation is of the form [17]

$$\frac{\partial h}{\partial t} + \frac{\partial}{\partial x}\left[\int_{-h}^{h} v_x dz\right] + \frac{\partial}{\partial y}\left[\int_{-h}^{h} v_y dz\right] = 0 \quad (2)$$

which, assuming symmetry about the midplane of the film, results in the following thin film equation:

$$\frac{\partial h}{\partial t} = \frac{2}{3\mu}\left(\frac{\partial}{\partial x}\left[h^3 \frac{\partial P}{\partial x}\right] + \frac{\partial}{\partial y}\left[h^3 \frac{\partial P}{\partial y}\right]\right), \quad (3)$$

where h is half the fluid film thickness (see Fig. 1) and no-slip boundaries are considered at $z=h$ and $-h$. The pressure consists of three parts, the first of which is due to the van der Waals interactions [15]

$$P_{vdW} = \frac{1}{6\pi}\left[\frac{A_{232}}{(2h)^3} - \frac{A_{123}}{(2h+d)^3} + \frac{A_{121}}{(2h+2d)^3}\right], \quad (4)$$

where A_{ijk} is the nonretarded Hamaker constant for media i and k interacting across media j, and d is the thickness of both the upper and lower solid capping layers. The pressure on the fluid due to the bending of the solid layers is of the form [26]

$$P_{bend} = \frac{Ed^3}{6(1-\sigma^2)}\left[\frac{\partial^4 h}{\partial x^4} + \frac{\partial^4 h}{\partial y^4} + \frac{\partial^4 h}{\partial x^2 \partial y^2}\right], \quad (5)$$

where E is the Young's modulus, and σ the Poisson's ratio, of the solid layers. The third, and final, pressure term accounts for the in-plane deformation of the film. The stretching free energy is given by [26]

$$H_s = \frac{Ed}{2(1+\sigma)}\int u_{xx}^2 + u_{yy}^2 + 2u_{xy}^2 + \frac{\sigma}{1-2\sigma}(u_{xx}+u_{yy})^2 d\Omega, \quad (6)$$

where

$$u_{ij} = \frac{1}{2}\left(\frac{\partial u_i}{\partial j} + \frac{\partial u_j}{\partial i} + \frac{\partial h}{\partial i}\frac{\partial h}{\partial j}\right)$$

is the strain tensor, including cross terms in h, Ω is the area of the film, and u_i is the displacement in the ith direction. The functional derivative of this free energy results in the following local pressure term:

$$P_s = \frac{Ed}{2(1+\sigma)}\left[\left(1+\frac{\sigma}{1-2\sigma}\right)\left(2\frac{\partial u_x}{\partial x}\frac{\partial^2 h}{\partial x^2} + 3\left(\frac{\partial h}{\partial x}\right)^2\frac{\partial^2 h}{\partial x^2}\right)\right.$$
$$+3\left(\frac{\partial h}{\partial y}\right)^2\frac{\partial^2 h}{\partial y^2} + \left(\frac{\partial h}{\partial x}\right)^2\frac{\partial^2 h}{\partial y^2} + 4\frac{\partial h}{\partial x}\frac{\partial h}{\partial y}\frac{\partial^2 h}{\partial x \partial y}$$
$$+\left(\frac{\partial h}{\partial y}\right)^2\frac{\partial^2 h}{\partial x^2} + \left(\frac{2\sigma}{1-2\sigma}\right)\left(\frac{1}{2}\left(\frac{\partial h}{\partial y}\right)^2\frac{\partial^2 h}{\partial x^2}\right.$$
$$\left.\left. +2\frac{\partial h}{\partial x}\frac{\partial h}{\partial y}\frac{\partial^2 h}{\partial x \partial y} + \frac{\partial u_x}{\partial x}\frac{\partial^2 h}{\partial y^2} + \frac{1}{2}\left(\frac{\partial h}{\partial x}\right)^2\frac{\partial^2 h}{\partial y^2}\right)\right]. \quad (7)$$

Terms involving u_y, and second derivatives of $\mathbf{u}$, are ignored in the above equation as in the systems considered here we limit the deformations to uniform, uniaxial strain fields in the x direction. Therefore, terms in the above equation contain-
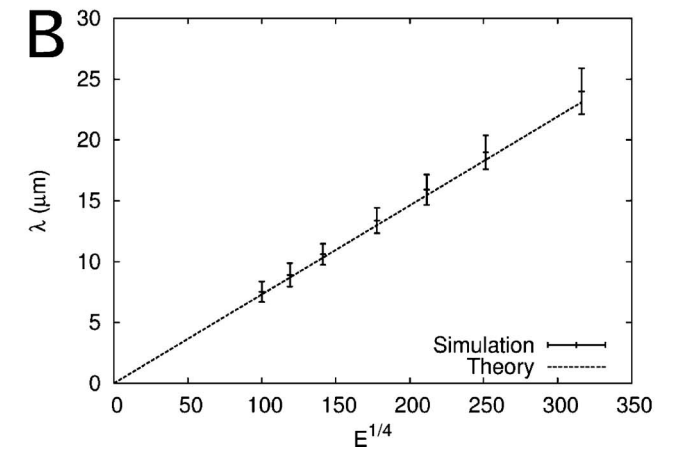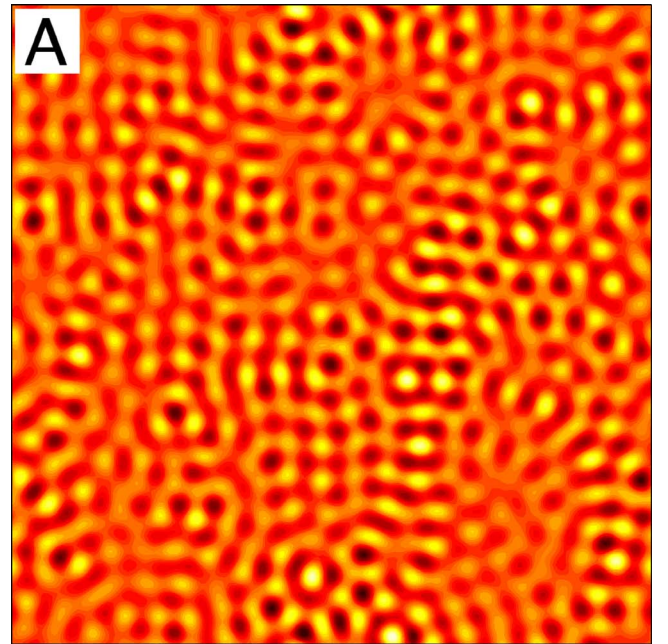
FIG. 2. (Color online) (a) A contour plot of Δh ranging from -1 nm (black) to 1 nm (white). The system size, laterally, is 256 μm $\times$ 256 μm, the Youngs modulus is 1 GPa and the snapshot is taken at time $t=585$ s. (b) Wavelength of surface undulations as a function of the Youngs modulus of the solid capping layers.
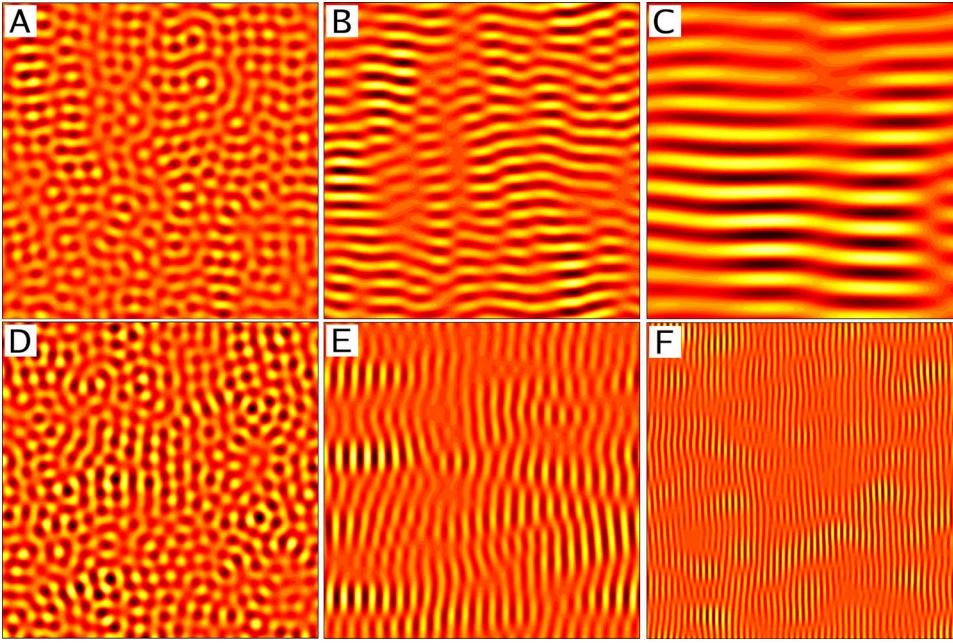
FIG. 3. (Color online) Contour plots of Δh, ranging from -1 nm (black) to 1 nm (white), for systems subject to externally applied strain fields of (a) 1×10^{-6}, (b) 1×10^{-5}, (c) 1×10^{-4}, (d) -1×10^{-6}, (e) -1×10^{-5}, and (f) -1×10^{-4}. The system size, laterally, is 256 μm $\times$ 256 μm, the Youngs modulus is 1 GPa and the snapshots are taken at times (a) $t=600$ s, (b) $t=750$ s, and (c) $t=2550$ s, (d) $t=570$ s, (e) $t=360$ s, and (f) $t=10.5$ s.

ing $\frac{\partial u_x}{\partial x}$ couple the application of a uniform and uniaxial strain field to forces acting perpendicular to the film. That is, we assume that the applied deformation is entirely confined to the x direction, and in this manner isolate the effects of a simple imposed deformation. The remaining terms are negligible until the deformation of the solid layers becomes comparable to their thickness. Therefore, not only can we simulate the evolution of the Dutcher film and include the van der Waals and elastic bending forces, we can also take into consideration an externally imposed deformation.

In the current study we take the Hamaker constants between the polymer solid and polymer fluid to be zero ($A_{232} = A_{123} = 0$) and consider only van der Waals forces from the capping layer-air interface ($A_{121} = 7.38 \times 10^{-20} J$). The initial half thickness of the fluid layer is $h(t=0) = h_0 + \epsilon$, where ϵ is a small random contribution and h_0 is 25 nm. The thickness of the solid capping layers is $d=25$ nm and the Poissons ratio of the solid layer is 0.3. The viscosity of the fluid influences the time scale of the problem and is taken to be $\mu = 10^4$ Pa s.

We solve the above set of equations using finite difference approximations. We use standard central difference approximations to capture the first and second order derivatives (forward and backward approximations are not necessary in the current model as we impose periodic boundary conditions in the x and y directions). The fourth order derivatives in Eq. (5) are approximated by the following map

$$\frac{\partial^4 h}{\partial x^4} + \frac{\partial^4 h}{\partial y^4} + \frac{\partial^4 h}{\partial x^2 \, \partial y^2}$$

$$= \frac{1}{\Delta x^4}[20h_{i,j} - 8(h_{i+1,j} + h_{i-1,j} + h_{i,j+1} + h_{i,j-1})$$

$$+ 2(h_{i+1,j+1} + h_{i-1,j-1} + h_{i+1,j-1} + h_{i-1,j+1})$$

$$+ h_{i+2,j} + h_{i-2,j} + h_{i,j+2} + h_{i,j-2}], \qquad (8)$$

where, $h_{i,j}$ is the height at the lattice coordinates i, j, and Δx is the lattice spacing, which is taken to be 1 μm. In this manner, we can solve the evolution equation, subject to the various pressures acting on the fluid layer.

In the absence of an applied strain field the undulations appear on the surface of the film as shown in Fig. 2(a), which depicts a contour plot of Δh. The system size, in lattice sites, is taken to be $L^2 = 256^2$ which corresponds to a system size of 256×10^{-12} m^2. Initially, the van der Waals forces destabilize small fluctuations on the surface of the film. The amplitude of these fluctuations grows exponentially with time throughout the simulation, whilst the domain size of the fluctuations grows to a characteristic value before plateauing. When the height variations are comparable to the thickness of the solid capping layers stretching contributions to the elastic energy become important. Localized compression and stretching in the lateral directions will then feed back into the evolution of the height variations and the combined stretching and bending elastic stresses will eventually be expected to balance the van der Waals pressures. However, for computational reasons we only simulate the initial growth of the undulations when height variations can be considered small compared to the film thickness and stretching contributions can be neglected [26]. That is, the displacement field in the x and y directions is not considered to be appreciably influenced by the local height variations and, in the absence of stretching and compression, we assume $\partial u_x / \partial x$ to be zero in Eq. (7). Figure 2(a) shows the height fluctuations at time $t \approx 10$ min, when the amplitude of the fluctuations is an order of magnitude smaller than the thickness of the solid capping layer. The undulations clearly self-assemble into domains of a characteristic wavelength, however, the orientation of the undulations would appear to be random.

The wavelength of the undulations is plotted in Fig. 2(b), as a function of the Young's modulus of the capping layers [27]. Increasing the Young's modulus results in solid capping layers which are less deformable and, therefore, the wave-

length of the undulations increases (undulations of larger wavelength involve less bending). Dutcher *et al.* [4] predicted that the fastest growing wavelength is given by $\lambda = 4\pi[\pi E/4A_{121}(1-\sigma^2)]^{1/4}d^{3/4}(h+d)$. In Fig. 2(b) we plot this theoretical prediction alongside our simulation results. Given that the theory considers one-dimensional corrugations, while clearly our systems exhibit isotropic two-dimensional undulations, it is promising that the comparison between our simulation results and theory is favorable. However, the theoretical analysis is based on the same continuum theories incorporated into our model and, therefore, such agreement is not surprising.

It would be highly desirable to exhibit some control over the direction of these undulations in order to tailor the surface topography towards specific applications. Figure 3 shows contour plots of various systems subject to uniaxial strain fields during the entire simulation. While we still assume height variations have a negligible effect on the lateral deformations, we now use Eq. (7) to incorporate the effects of the *imposed* deformations (either stretching or compression) which is shown to have an appreciable influence on the evolution of the height variations. In Figs. 3(a)–3(c) the systems are stretched in the x direction with uniaxial strain fields of the magnitude 1×10^{-6}, 1×10^{-5}, and 1×10^{-4}, respectively. At the lowest strain field considered the morphology appears to be largely unaffected by the applied strain. However, as the strain field is increased the wrinkled morphology begins to orient in the tensile direction. Furthermore, the periodicity of the undulations appears to increase with increased stretching. The applied strain appears to be *suppressing* the growth of fluctuations in the tensile direction resulting in a topography consisting solely of corrugations perpendicular to the tensile direction. Figures 3(d)–3(f) show the height variations in systems which are compressed with uniaxial strain fields of the magnitude 1×10^{-6}, 1×10^{-5}, and 1×10^{-4}, respectively. Rather than suppressing the growth of undulations, as in the stretched systems, compression *encourages* the growth of fluctuations [28]. This results in corrugated morphologies running perpendicular to the compression direction. Similar to the effects of stretching, compressing the systems also influences the periodicity of the corrugations. Systems under compression, however, exhibit corrugations of smaller wavelengths than that of equivalent undeformed systems.

It is interesting that the wavelengths depend not only on the initial thicknesses of the layers, the elastic properties of the solid capping layers, and the strength of the van der Waals forces, but also on the nature of the applied deformations. In order to quantify these effects we plot the relative wavelength of the corrugations against the magnitude of the strain field (see Fig. 4). The relative wavelength of the corrugation is defined as $(\lambda-\lambda_0)/\lambda_0$, where λ_0 is the wavelength of undulations in the undeformed systems. Stretching the films can result in an increase in the periodicity of up to
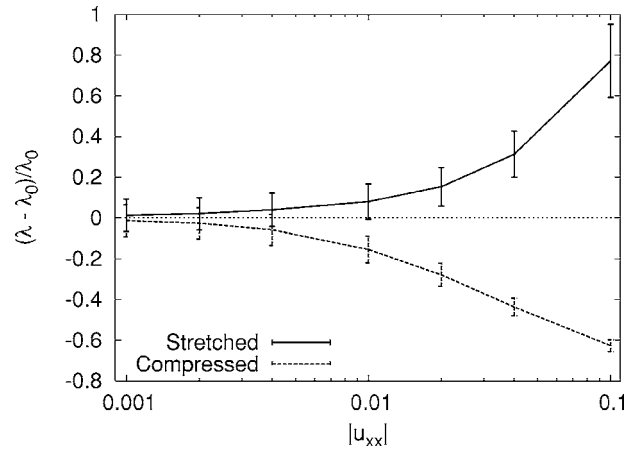
FIG. 4. Relative wavelength of surface corrugations as a function of the magnitude of the applied strain field.

80%, while compressing the films can results in a decrease of up to 60%, for the systems considered here. Therefore, not only does deforming the films result in highly anisotropic corrugations extending over the entire system, but the wavelength of these corrugations can also be finely tuned.

To summarize, we have augmented a thin film equation of fluid flow with pressure terms from elasticity theory in order to describe the spontaneous formation of undulations in Dutcher films. These simulations capture the dynamics of undulation growth in these systems and the *selection* of a characteristic wavelength. Furthermore, we find the wavelength of these undulations to be in quantitative agreement with theoretical predictions. We subject the films to uniaxial deformations and observe that the direction and periodicity of the undulations can be manipulated to create highly anisotropic corrugated morphologies.

It is worth noting that local anisotropy is often observed in experimental systems [4,6], whilst in the undeformed systems considered here the undulated morphologies are isotropic. This suggests that residual strains are present in the experimental films, as a consequence for example of thermal mismatch between the sample and holder. Manipulation of these strains could result in the formation of corrugations in a given direction over large areas.

The results presented here are for when the height variations are of small amplitude and have a negligible effect on the lateral deformations. Future studies will attempt to include these contributions and simulate larger deformations. It is anticipated that the stretching term could have an effect on the wavelength of the correlations at later times, just prior to the two layers meeting. Once the two solid layers meet, however, the system will seek to maximize the contact between the two layers (and decrease the overall van der Waals energy of the system). This could potentially result in the formation of isolated circular pockets of fluid.

[1] M. Ibn-Elhaj and M. Schadt, Nature (London) **410**, 796 (2001).

[2] R. Windisch, P. Heremans, A. Knobloch, P. Kiesel, G. H. Dohler, B. Dutta, and G. Borghs, Appl. Phys. Lett. **74**, 2256 (1999).

[3] T. Nishikawa, J. Nishida, R. Ookura, S. I. Nishimura, S. Wada, T. Karino, and M. Shimomura, Mater. Sci. Eng., C **8-9**, 495 (1999).

[4] K. Dalnoki-Veress, B. G. Nickel, and J. R. Dutcher, Phys. Rev. Lett. **82**, 1486 (1999).

[5] J. R. Dutcher, K. Dalnoki-Veress, B. G. Nickel, and C. B. Roth, Macromol. Symp. **159**, 143 (2000).

[6] C. A. Murray, S. W. Kamp, J. M. Thomas, and J. R. Dutcher, Phys. Rev. E **69**, 061612 (2004).

[7] N. Bowden, S. Brittain, A. G. Evans, J. W. Hutchinson, and G. M. Whitesides, Nature (London) **393**, 146 (1998).

[8] P. J. Yoo, K. Y. Suh, S. Y. Park, and H. H. Lee, Adv. Mater. (Weinheim, Ger.) **14**, 1383 (2002).

[9] T. Ohzono and M. Shimomura, Phys. Rev. E **72**, 025203(R) (2005).

[10] N. Sridhar, D. J. Srolovitz, and Z. Suo, Appl. Phys. Lett. **78**, 2482 (2001).

[11] C. Li, X. Zhang, and Z. Cao, Science **309**, 909 (2005).

[12] J. S. Sharp and R. A. L. Jones, Adv. Mater. (Weinheim, Ger.) **14**(11), 799 (2002).

[13] M. D. Morariu, E. Schäffer, and U. Steiner, Phys. Rev. Lett. **92**, 156102 (2004).

[14] M. Müller-Wiegand, G. Georgiev, E. Oesterschulze, T. Fuhrmann, and J. Salbeck, Appl. Phys. Lett. **81**, 4940 (2002).

[15] J. Israelachvili, *Intermolecular and Surface Forces* (Academic Press, London, 1992).

[16] M. B. Williams and S. H. Davis, J. Colloid Interface Sci. **90**, 220 (1982).

[17] A. Oron, S. H. Davis, and S. G. Bankoff, Rev. Mod. Phys. **69**, 931 (1997).

[18] P. J. Yoo and H. H. Lee, Macromolecules **38**, 2820 (2005).

[19] A. Sharma and R. Khanna, Phys. Rev. Lett. **81**, 3463 (1998).

[20] A. Oron, Phys. Rev. Lett. **85**, 2108 (2000).

[21] J. Becker, G. Grün, R. Seemann, H. Mantz, K. Jacobs, K. R. Mecke, and R. Blossey, Nat. Mater. **2**, 59 (2003).

[22] R. Konnur, K. Kargupta, and A. Sharma, Phys. Rev. Lett. **84**, 931 (2000).

[23] A. Sharma and J. Mittal, Phys. Rev. Lett. **89**, 186101 (2002).

[24] N. Clarke, Macromolecules **38**, 6775 (2005).

[25] H. Schlichting, *Boundary-Layer Theory* (McGraw-Hill, New York, 1979).

[26] L. D. Landau and E. M. Lifshitz, *Theory of Elasticity* (Pergamon Press, Oxford, 1970).

[27] The wavelength is obtained from the first moment of the radially averaged fast Fourier transform (FFT) of the height variations. The FFT is averaged over three independent simulations. The error bars reflect the standard deviation and are obtained from the second moment of the radially averaged FFT.

[28] It should be noted that thin plates subject to compressive stresses can buckle regardless of the van der Waals interactions. We can probe this buckling by turning off the van der Waals interactions in our simulations. We find that the buckling occurs on times scales at least an order of magnitude larger than that of van der Waals induced fluctuation growth for the systems subjected to a compressive strain of 1×10^{-5}. However, for the systems subjected to a compressive strain of 1×10^{-4} the time scales are equivalent and, therefore, both fluctuation growth due to van der Waals interactions and buckling due to the applied compressive strain field are expected to play a part in the final morphology.